KECK Geology Consortium
Learning Science Through Research
Published by the Keck Geology Consortium
Short Contributions
Keck Geology Consortium
Volume 35
May 2023
doi: 10.18277/AKRSG.2023.35.02

MODELING FAULT-RELATED FRACTURING ASSOCIATED WITH A SEGMENTED NORMAL FAULT: IMPLICATIONS FOR GEOTHERMAL ENERGY POTENTIAL

AUDREY JENNINGS, Trinity University
Project Advisor: Benjamin Surpless

INTRODUCTION

Geothermal energy is a growing source of renewable energy in the United States, but it can be both technically challenging and financially risky to identify locations with high potential (e.g., Micale et. al., 2014). In order for a geothermal system to be conducive to any utility-scale electricity or heat generation, it must have high heat levels and pathways for fluid to flow. Faulting, which deforms rock and creates fluid pathways, can create an ideal scenario for geothermal energy production. By analyzing stress and strain distributions in certain fault zones, we may be able to locate productive systems. Faulds and Hinz (2015) describe high-density fracturing around segmented normal faults in extensional settings, making these zones promising for geothermal energy production. To explore the geothermal potential in segmented fault zones, I built 3D fault models in Move 2020 (by Petex) to assess displacement, stress, strain, and fracturing at different stages of fault interaction, which we compare to field data from the Sevier fault zone in southern Utah.

The Sevier fault zone is a NW-striking, segmented normal fault system that exhibits varying stages and types of fault segment interactions, including relay ramps and transfer zones that are associated with high-intensity fracturing (Surpless and McKeighan, 2022). Given the presence of these fracture-conducive geologic settings, we constructed 3D Move models based on the Sevier system in order to predict how vertical displacement, stress, strain, fracture orientation, and fracture intensity develop within a segmented, progressively overlapping normal fault system. With our work, we can investigate how fault segmentation and linkage affect stress and strain within a fault zone, and how stress and strain in these systems might evolve over time. We also can more definitively determine the effects of fault-related stress and strain on fracturing orientations and intensities within a given rock volume, as well as how stress, strain, and fracturing intensities and orientations evolve as fault segments propagate past each other. Finally, using both our modeling results and collected field data, we aim to develop new strategies for how to best utilize 3D modeling as a tool to efficiently identify locations with high geothermal potential, so that they can be targeted for further investigation.

BACKGROUND

At their most basic, geothermal systems require two primary factors: heat and flowing fluids. Heat flow has previously been well-mapped, indicating locations where geothermal energy may be possible (Boden, 2017). Geothermal systems tend to be productive at locations with average temperatures above 100 degrees C, but due to their subsurface location, identifying fluid flow pathways that will be conducive to geothermal systems can be much more difficult (e.g., Boden, 2017). Metrics to evaluate fluid flow potential include porosity and permeability. In general, highly permeable materials support geothermal systems, since connected open spaces allow for fluids to flow at high rates. However, permeability due to rock fracturing is especially important to identify when considering geothermal energy system viability, since fracture permeability can often be many orders of magnitude greater than matrix permeability. Given that researchers estimate that productive geothermal

systems must average a fluid flow rate of 200 kg/s, porosity simulation models predict that a fracture permeability of local material between 0.05 and 0.5 darcies is necessary to sustain a productive flow rate (1 darcy = volumetric flow rate of 1 cm^3/s of water with a viscosity of 1 centipoise over a cross-sectional area of 1 cm^2 under a pressure gradient of 1 atmosphere per centimeter) (e.g., Boden, 2017). Thus, identifying settings with high-level rock fracturing that produce permeability in these ranges will be key to establishing utility-scale geothermal energy production.

One promising location for geothermal energy is the Sevier fault zone in southern Utah. The Sevier fault has accommodated extensional strain between the Basin and Range Province and the Colorado Plateau since the Miocene (e.g., Surpless and McKeighan, 2022), and is a segmented normal fault that dips steeply to the west and exhibits 600 to 700 m of dip-slip displacement. Overlapping fault segments have led to complex structures, including relay ramps, fracture zones, and tip, wall, and linkage damage zones (e.g., Davis, 1999; Hecker, 1993; Smith and Arabasz, 1999). These types of structures are consistent with structural settings where geothermal systems form (e.g., Curewitz and Karson, 1997; Faulds and Hinz, 2015). Localities that exhibit combinations of these settings, which we have documented along the Sevier fault, suggest that the Sevier fault is a promising location for understanding how and where high-geothermal potential systems develop. Of the structural settings commonly linked to high geothermal potential, two that are especially common within segmented normal fault systems are the regions between interacting fault tips and across relay ramps. As fault tip stress zones approach one another, they may begin to interact and cause new deformation (Fig. 1). Such "transfer zones" can result in the development of relay ramps, structures that connect the hanging wall of one fault segment to the footwall of another segment and help facilitate the transfer of strain and slip between the two segments (Fig. 2).

Relay ramp formation depends on the specific geometry and relationship between involved fault segments; if segments are too far apart, they will not interact. If segments are more closely spaced, as

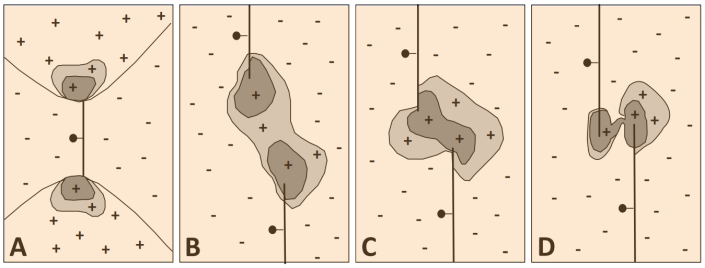

Figure 1. Map view of lateral fault segment propagation and associated stress field changes (elevated stress shown in gray and dark gray. - symbols correspond to areas where failure is not likely to occur as the fault continues to propagate. Diagram A modified from Cowie and Shipton (1998), and diagrams B - D modified from Crider and Pollard (1998) and Crider (2001).

segments propagate past each other, deformation in stress transfer zones and along relay ramps increase, and the relay ramp may become breached, physically linking the two fault segments into one system (Fig. 2) (e.g., Trudgill and Cartwright, 1994; Crider and Pollard, 1998). Importantly, spacing and geometry of faults affect whether fault linkage occurs and ultimately how fault linkage occurs. Fault dip and the subsurface distance between fault tip lines most strongly affect the likelihood of linkage (Crider and Pollard, 1998). Linkage of overlapping faults typically includes an interaction phase during which a relay ramp forms due to stress field interactions between faults (e.g., Crider, 2001; Crider and Pollard, 1998). Relay ramps connect the hanging wall of one fault segment to the footwall of another segment, effectively transferring strain and/or slip between the two segments, and may ultimately directly link the faults to form a single segmented fault (e.g., Larsen,

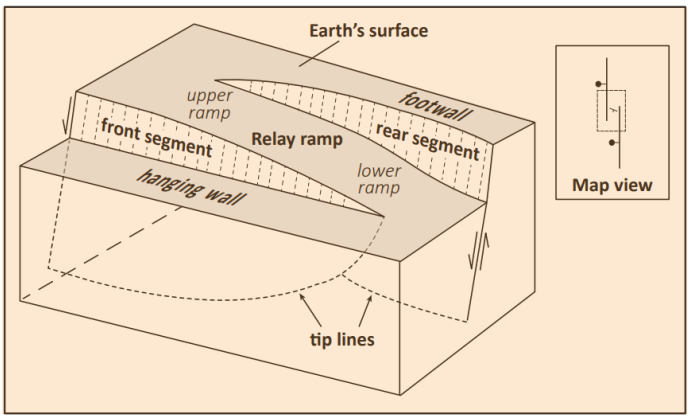

Figure 2. Diagram of a relay ramp developing between en echelon normal fault segments. Within the fault scarps, fault slip tapers to zero at the tips. The insert shows a map view of the relay ramp, with the fault segments represented by parallel lines and the dashed box indicating the location of the 3D diagram. Figure modified from Trudgill and Cartwright (1994) and Crider and Pollard (1998).

1988; Morley et al., 1990; Peacock and Sanderson, 1991; Trudgill and Cartwright, 1994; Crider and Pollard, 1998; Faulds and Varga, 1998; Walsh et al., 1999; Peacock et al., 2000; Ferrill and Morris, 2001; Reber et al., 2001; Camanni et al., 2019).

METHODS

The Fault Response Modeling (FRM) module of Petex's Move 2020 modeling software calculates variables including displacement, strain, and stress within a user-defined fault system using elastic dislocation theory calculations at "sampling" points within a user-defined medium (Petex, 2020). With the FRM module, we created a total of 16 fault models mimicking a segmented normal fault system, based on the geometry of the Sevier fault zone. A simplified description of the modeling process and the lithological conditions of the observation layer are presented in Fig. 3 and Table 1, respectively. The fault model consists of two parallel en echelon fault segments, each ten kilometers long, 1 kilometer apart, and dipping 70 degrees. This configuration approximates the observed geometry of interacting fault segments within the real Sevier fault zone. In order to mimic simultaneous vertical throw and horizontal displacement, we assigned progressive amounts of displacement (of 5, 25, 50, and 150 m) to four models that also experienced progressive lateral propagation. Thus, a model with two laterally separated fault segments (such that no interaction occurred between them) experienced 5 m of slip, a model with the fault segment tips placed even with one another experienced 25 m of slip, a model with 1 km of overlap between fault segments experienced 50 m of slip, and a model with 3 km of overlap between fault segments experienced 150 m of slip.

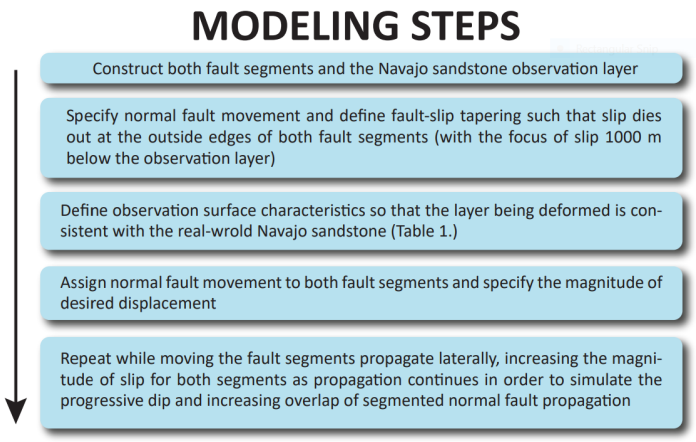

Figure 3 . Workflow for creating 3D models of the Sevier fault zone in the Fault Response Modeling module of MOVE 2020.

Table 1. Rock and fault properties used in this study.

NAVAJO SANDSTONE PROPERTIES	
POISSON'S RATIO	0.25
YOUNG'S MODULUS	30,000 MPa
COEFFICIENT OF FRICTION	0.40
FRICTION ANGLE	30 degrees
COHESION	2.00 MPa
DENSITY	2,459 kg/m³

FAULT PROPERTIES	
FREE SURFACE ELEVATION	0.0 m
DEPTH OF MAXIMUM SLIP	-1,000 m
DISPLACEMENT	Defined by slip
OPENING SLIP MAGNITUDE	0.0 m
DIP ANGLE	70 degrees

These slips occurred along an elliptical displacement gradient on the fault plane, with the greatest amount of slip equidistant from the fault tips and at 1 kilometer below the observation surface, and 0 slip at the fault tips. Such dimensions meant that the slip occurred across the "no interaction" model at a gradient of 1 m/km, across the "even" model at a gradient of 5 m/km, across the "1 km overlap" model at a gradient of 10m/km, and across the "3 km overlap" model at a gradient of 30 m/km from the foci to the fault tips. We generated 16 models showing vertical displacement, maximum coulomb shear stress, strain dilation, and predicted fracture intensity and orientation based on the 4 given fault configurations. Though our models do not precisely match the fault geometry of the Sevier or the complete stratigraphy, they do represent the general fault interactions within the system and therefore can be used to gain better insight into the distribution of fracturing and enhanced permeability within the Sevier fault zone. By comparing our modeled results to the fracture networks documented along the Sevier fault zone (Nishimoto, this volume), we can validate our modeling process and draw general conclusions about faulting and fracturing within segmented normal fault systems.

RESULTS

Our modeling results reveal how vertical displacement, stress, strain, fracture orientation, and fracture intensity vary across a range of total

displacements and fault geometries (Fig. 4). Model results are shown with a heatmap, with values increasing from the lowest (shown in blue), to the highest (shown in red). Fault geometry affects the distribution of throw, stress, strain, and fracturing across models with progressive displacement and relative overlap. The fault segments show two separate stress fields in the "no interaction" model, but the fields begin to converge with the "even" model and continue to do so as the segments become increasingly overlapped. Since the models mimic the Sevier fault zone, rather than perfectly replicating it, we cannot use the models to predict specific throw, stress, and strain values; however, we can use these values for general comparisons between models. Thus, it appears that stress and strain values increase as fault segment overlap progresses. In the greatly overlapped model (with 3 km of overlap and 150 m of slip), calculated maximum Coulomb shear stress values reach a maximum of 186.3 MPa along the fault plane; in the no-interaction model experiencing 5 m of slip, the maximum calculated maximum Coulomb shear stress value occurs along the fault plane as well, but only at 0.9 MPa. Strain dilation varies similarly, with the maximum strain dilation value recorded as 0.000 in the no-interaction model and 0.0011in the 3 km overlap model, occurring in all models near the fault tips and in the hanging wall (HW) of the system.

Even within individual models, throw, stress, strain and fracturing vary across parts of the fault system. For all of our models, stress and strain are largely concentrated at the fault tips, and overall stress is greatest in the footwall while strain is greatest in the hanging wall. Our models also show high-intensity fracturing concentrated at fault tips and in the hanging wall of fault systems. Fractures are generally oriented parallel to the fault segment(s) in the hanging wall, and more perpendicular to the fault in the footwall. At the tips, where strain is greatest and stress fields are

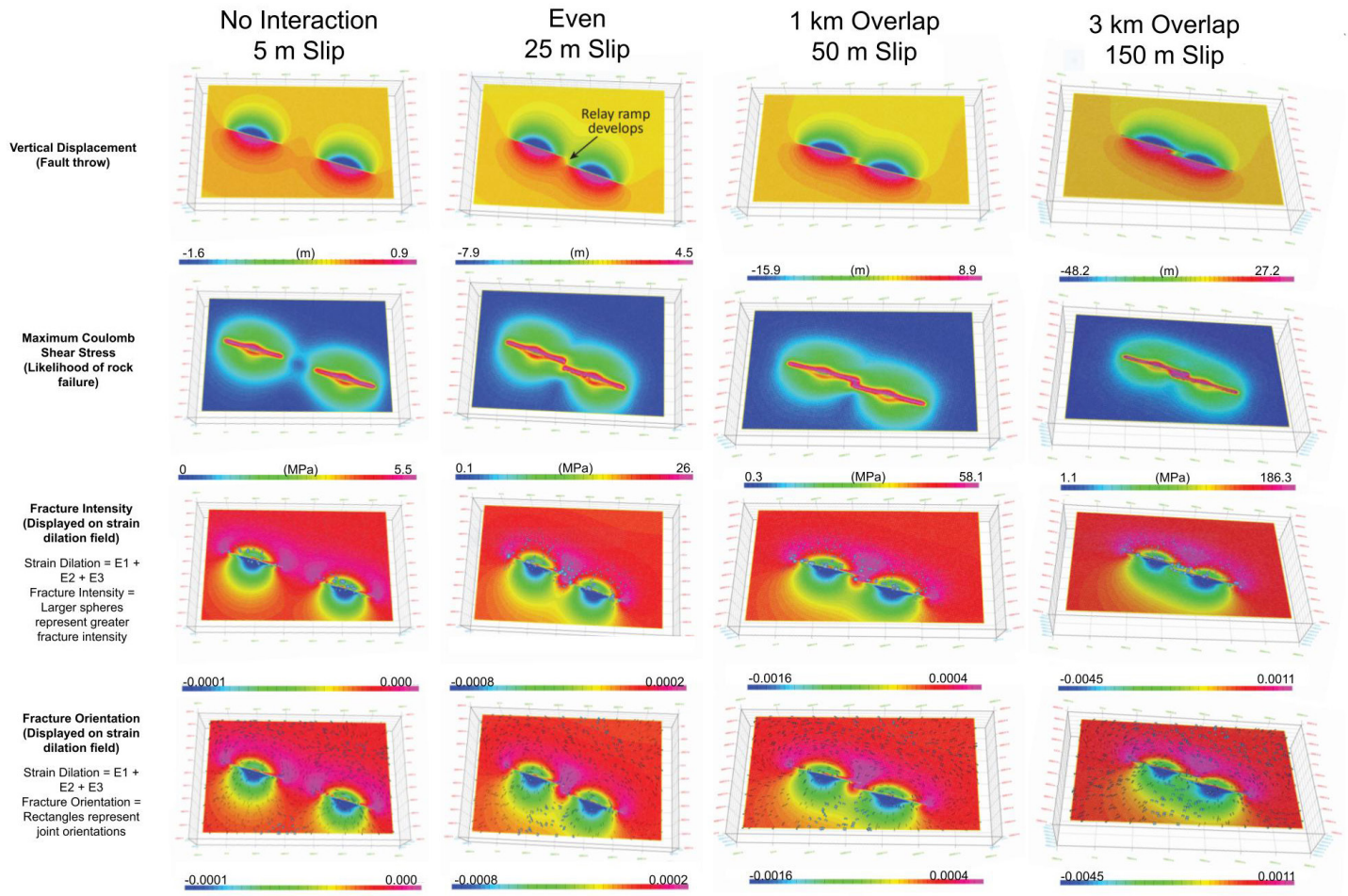

Figure 4. Modeling results, showing vertical displacement, maximum coulomb shear stress, strain dilation, fracture intensity, fracture orientation.

interacting between segments, the fracture orientations are much more variable than in the midsection of the fault system.

In addition, prior modeling of fault interactions reveal that the greatest Coulomb stress occurs along the relay zone between fault segments where tips of the different segments are closest (Crider and Pollard, 1998). Our results support these findings, with yellow lines on the models representing higher maximum stress and strain from the northernmost tip of the western segment to the northernmost tip of the eastern segment. Strain generates fractures in rock in alignment with our models which show high-intensity fracturing at fault tips where strain is concentrated. However, fault segments with extreme overlap experience less shear Coulomb stress relative to applied load when compared to underlapped fault segments (Crider and Pollard, 1998), so the increase in maximum stress within the relay zone in our overlapped model is relatively small.

DISCUSSION

Our results indicate that segmented normal fault systems with significant levels of overlap between fault segments present a promising location for further geothermal investigation due to the higher intensity fracturing present, relative to single or underlapped systems. Specifically, fracturing intensity appears especially elevated between overlapped fault tips (at mid-to-high levels of vertical displacement) as well as along relay ramp development zones between fault tips. These locations have also been identified as having especially high stress and strain in prior fault-linkage models with similar geometries (Crider and Pollard, 1998). Given the strong relationship between high levels of stress, strain, and elevated fracture intensity, our models seem to support Crider and Pollard's (1998) analysis of high-stress and strain areas in fault linkage systems and also indicate that such locations may be high in geothermal energy potential. From our models, it also appears that the hanging wall of segmented normal fault systems (with higher fracture intensities than the footwall) demonstrate more promise for fluid flow and thus geothermal energy. Targeting further geothermal research in such geological formations could be an important step in finding new ways to harness the Earth's heat, and further encourage both public and private investment in geothermal projects (e.g., Micale et. al., 2014). However, applying the proper geothermal energy system to the geological constraints of the specific fault zone will be critical to properly using any local potential.

Our models indicate that the intensities and orientations of subsurface fracturing that would be conducive to geothermal energy are likely present within the overlapped, normal Sevier fault zone, but the temperature levels within this specific fault system are likely too low or too inconsistent to provide usable geothermal electricity given current geothermal infrastructure (Boden, 2017). However, we can generalize the displacement, stress, strain, and fracturing patterns we see in our models to other segmented normal fault systems that are in geothermally warmer or more accessible regions, using our data to indicate where within such systems we may expect to see the greatest potential and what factors (like fault geometry or amount of slip) contribute most greatly to the development of geothermal potential. Ultimately, the relative agreement between our fracture modeling results and the damage zone data collected during fieldwork along the Sevier fault (Nishimoto, this volume) illustrates the potential for 3D modeling to help identify regions with high geothermal potential. Given that one main obstacle to expanding geothermal energy is the difficulty in identifying high-potential geothermal systems, improving modeling strategies for predicting the fracturing intensity and thus fluid flow potential of different geologic settings is an important step in making utility-scale geothermal energy a feasible future solution.

ACKNOWLEDGMENTS

This material is based upon work supported by the Keck Geology Consortium and the National Science Foundation under Grant No. 2050697. It was also supported by NSF Award 2042114 to PI Surpless. Finally, funding was provided by the Geosciences Department at Trinity University, including funding from the Roy and Tinker Funds to support undergraduate student research.

REFERENCES

Boden, D.R., 2017, Geologic Fundamentals of Geothermal Energy: Boca Raton, Florida, CRC Press, 399 p.

Cowie, P.A., and Shipton, Z.K., 1998, Fault Tip Displacement Gradients and Process Zone Dimensions, Journal of Structural Geology, v. 20, p. 983 - 997.

Crider, J., 2001, Oblique Slip and the Geometry of Normal-Fault Linkage: Mechanics and a Case Study from the Basin and Range in Oregon, Journal of Structural Geology, v. 23, 12, p. 1997 - 2009.

Crider, J., and Pollard, D., 1998, Fault linkage: Three-dimensional mechanical interaction between echelon normal faults, Journal of Geophysical Research, v. 103, p. 24.373 - 24.391.

Curewitz, D., and Karson, J. A., 1997, Structural settings of hydrothermal outflow: Fracture permeability maintained by fault propagation and interaction, J. Volcanol. Geotherm. Res., v. 79, p. 149 - 168.

Davis, G.H., 1999, Structural geology of the Colorado Plateau region of southern Utah: Geological Society of America Special Paper 342, p. 127.

Doelling, H.H., 2008, Geologic map of the Kanab 30'x60' quadrangle, Kane and Washington Counties, Utah, and Coconino and Mohave Counties, Arizona, 1:100,000-scale: Utah Geological Survey, MP-08-2DM

Faulds, J., and Hinz, N., 2015, Favorable Tectonic and Structural Settings of Geothermal Systems in the Great Basin Region, Western USA: Proxies for Discovering Blind Geothermal Systems, in Proceedings, World Geothermal Congress, Melbourne: Australia, Nevada Bureau of Mines and Geology (https://www.osti.gov/servlets/purl/1724082).

Hecker, S., 1993, Quaternary tectonics of Utah with emphasis on earthquake-hazard characterization: Utah Geological Survey Bulletin, v. 127, p. 1 - 31.

Micale, V., Oliver, P., and Messent, F., 2014, The Role of Public Finance in Deploying Geothermal: Background Paper, in San Giorgio Group Report, Climate Policy Initiative, p. 1 - 15.

Petex, 2020, Move 2020 Tutorial 33: Fault Response Modeling.

Schiefelbein, I., 2002, Fault segmentation, fault linkage, and hazards along the Sevier fault, southwestern Utah [M.S. thesis]: Las Vegas, University of Nevada at Las Vegas, 132 p.

Smith, R.B., and Arabasz, W.J., 1991, Seismicity of the Intermountain Seismic Belt, in Slemmons, D.B., Engdahl, E.R., Zoback, M.D., and Blackwell, D.D., eds., Neotectonics of North America: Geological Society of America, p. 185 - 228.

Schultz, R., 2010, Porosity and Grain Size Controls on Compaction Band Formation in Jurassic Navajo Sandstone: American Geological Union geophysical Research Letters v. 37, 22.

Surpless, B.E., and McKeighan, C., 2022, The role of dynamic fracture branching in the evolution of fracture networks: an outcrop study of the Jurassic Navajo Sandstone, southern Utah: Journal of Structural Geology, v. 161. DOI: 10.1016/j.jsg.2022.104664.

Trudgill, B., and Cartwright, J., 1994, Relay-Ramp Forms and Normal-Fault Linkages, Canyonlands National-Park, Utah. Geological Society of America Bulletin, v. 106, p. 1143 - 1157.